Available online at www.sciencedirect.com
SCIENCE DIRECT®
International Journal of Heat and Mass Transfer 48 (2005) 3932–3944
International Journal of HEAT and MASS TRANSFER
www.elsevier.com/locate/ijhmt

Analysis of melting and resolidification in a two-component metal powder bed subjected to temporal Gaussian heat flux

Chad Konrad, Yuwen Zhang *, Bin Xiao

Department of Mechanical and Aerospace Engineering, University of Missouri—Columbia, Columbia, MO 65211, USA

Received 10 December 2004; received in revised form 15 April 2005
Available online 28 June 2005

Abstract

Melting and resolidification of a subcooled, two-component metal powder bed subjected to temporal Gaussian heat flux is investigated analytically in this paper. The integral approximate solutions for preheating, melting with shrinkage, and resolidification are obtained. An increase in heat source intensity or powder bed porosity will result in an increase of the melt pool depth, melt pool temperature, and the overall processing time. The melt pool becomes shallower with increasing subcooling because more heat flux is needed to melt the powder. A change in the liquid phase porosity will increase the process time only slightly and have a negligible effect on the amount of melted material produced.

1. Introduction

Selective laser sintering (SLS) is an emerging technology that can build structurally sound parts from powdered material via layer-by-layer sintering (for amorphous powder, such as polycarbonate) or melting (for crystalline powder, such as metal) induced by a directed laser beam. Fabrication of metal parts is a very challenging task since the temperature required to bind the metal powder particles is much higher than that needed to bind the amorphous powder particles. SLS is a very useful rapid manufacturing method because it allows for the manufacture of complex parts often unobtainable by more common manufacturing processes [1,2]. During the SLS process the surface of a powder bed is scanned with a laser heat source to melt the powder and as the beam moves away the liquid resolidifies into a solid. Another layer of powder is then pushed over the newly solidified surface and the process is repeated, thus building a solid object layer by layer.

Recent advances in metallic SLS have improved the technology, but it still remains limited in terms of material versatility, quality, and precision [3]. The behaviors of the powders used in SLS processes are quite different depending on the material, the shape and size of powder particles and so on, and it is necessary to use a trial and error method to find suitable materials for an SLS process [4]. It is for these reasons that a sound theoretical SLS model must be developed so that the results of SLS techniques and the quality of the parts can be predicted accurately.

There are other obstacles that must also be overcome before SLS can be used for mass production of final, high quality parts that exhibit good surface finish and

* Corresponding author.
E-mail address: zhangyu@missouri.edu (Y. Zhang).

0017-9310/$ - see front matter © 2005 Elsevier Ltd. All rights reserved.
doi:10.1016/j.ijheatmasstransfer.2005.04.010

Nomenclature

h_{sl}	latent heat of fusion [J kg^{-1}]
k	thermal conductivity [W m^{-1} °C^{-1}]
K	dimensionless thermal conductivity
q''	heat flux [W m^{-2}]
s	solid–liquid interface location [m]
s_0	location of liquid surface [m]
S	dimensionless solid–liquid interface location
S_0	dimensionless location of liquid surface
Sc	subcooling parameter
Ste	Stefan number
t	time [s]
t_p	half width of the laser beam pulse at $1/e$ [s]
T	temperature [°C]
w	velocity of liquid phase [m s^{-1}]
W	dimensionless velocity of the liquid phase
z	coordinate [m]
Z	dimensionless coordinate

Greek symbols

α	thermal diffusivity [m^2 s^{-1}]
$\bar{\alpha}$	dimensionless thermal diffusivity
δ	thickness of thermal layer [m]
Δ	dimensionless thickness of thermal layer
ε	volume fraction of gas(es) (porosity for unsintered powder)
θ	dimensionless temperature
ρ	density [kg m^{-3}]
τ	dimensionless time
ϕ	volume fraction of the low melting point powder in the powder mixture

Subscripts

0	beginning (when preheating begins)
final	final (when solidification ends)
g	gas(es)
H	high melting point metal
i	initial
l	liquid phase (mixture of low melting point metal liquid and high melting point powder solid)
L	low melting point powder
m	melting point (when melting begins)
p	fully densified resolidified part
r	resolidified part
s	unsintered solid (mixture of two solid powders)
sol	solidification (when solidification begins)

desirable mechanical properties. One such obstacle is the balling phenomenon [5], in which melted powder grains stick to each other via surface tension forces, thereby forming a series of spheres with diameters approximately equal to the diameters of the laser beam. The balling phenomenon is well documented, an extensive study of which can be found in Tolochko et al. [5]. There are several ways the balling phenomenon can be combated, one of which is to use a powder bed consisting of two different types of metal powder, one with a significantly higher melting point than the other as suggested by Bunnell [6] and Manzur et al. [7]. If such a mixture is used the higher melting point powder will not melt, breaking up the surface tension forces and forcing out the interstitial gasses as desired. Another way to minimize the balling effect is to use a pulsed laser to decrease the life span of the melt pool and thus help avoid the balling effect [8].

Since melting and resolidification are the mechanisms of this laser-based metal part manufacturing technique their inclusion in any SLS model for metal powder is essential. The fundamentals of melting and solidification have been investigated extensively [9,10], however, laser-induced melting of metal powder in SLS processes differs from conventional melting because the subcooled powder can consist of as much as 40–60% gas. During melting it is necessary for the liquid phase to collect and drive the interstitial gasses out of the powder bed, effectively "shrinking" the volume of the powder bed. It is because of this shrinkage phenomenon that the powder bed experiences a significant density change during the melting process, resulting in motion of the surface of the powder bed during the SLS process.

Zhang and Faghri [11] analytically solved a one-dimensional melting problem in a semi-infinite two-component metal powder bed subjected to *constant* heat flux. The effects of the porosity of the loose powder and liquid, initial subcooling parameter, and dimensionless thermal conductivity of the interstitial gas were investigated. Chen and Zhang [12] obtained the analytical solution of melting in a two-component powder layer with finite thickness subject to *constant* heat flux. The effects of the porosities, Stefan number, and subcooling on the surface temperature and solid–liquid interface were investigated. In order to discover the advantages of utilizing a pulsed laser in a SLS process, melting and resolidification of a two-component metal powder bed of infinite thickness exposed to temporal Gaussian heat flux will be investigated. The governing equations will be nondimensionalized and the effect of a change in each of the independent parameters will be investigated. This paper represents a fundamental study of the SLS process upon which more comprehensive models may be based on in the future.

2. Physical model

Melting and resolidification of a bed of powder particles subjected to temporal Gaussian heat flux from a laser beam will be modeled in this paper. The diameter of the metal powder particles is much smaller than the diameter of the laser beam, which is in turn much smaller than the final desired part. The physical model of melting and resolidification is shown in Fig. 1. The initial temperature of the powder bed of infinite thickness, which contains two metal powders with significantly different melting points, is well below the melting temperature of the low melting point metal powder component. The origin of time is chosen to be the time at which the heat flux is at its maximum, thus the time-dependent heat flux is

$$q''(t) = q''_0 e^{-\frac{t^2}{t_p^2}} \tag{1}$$

The laser–powder bed interaction can be divided into three stages: (1) preheating, (2) melting with shrinkage, and (3) resolidification. During the preheating period the powder bed must absorb a significant amount of heat to bring the powder bed surface temperature up to the melting temperature of the low melting point powder, T_m. The duration of the preheating stage is defined as the time it will take for the surface temperature to reach to T_m. The melting stage begins after the surface temperature of the powder bed has reached the melting temperature of the low melting point powder. During this period the powder melts rapidly and consolidates into a liquid pool. This consolidation results from the fact that the liquid cannot maintain the relatively high initial porosity of the solid powder bed and therefore the interstitial gases are driven out of the liquid pool. This consolidation of the powder bed results in a significant density change, and thus liquid surface motion. The resulting liquid pool is not fully dense, in other words some interstitial gas is still trapped within the liquid phase, because the liquid lifetime is very short. It should be restated that the metal with the higher melting point will not melt during the entire process. The surface heat flux will reach its maximum at time $t = 0$, after which the heat flux will begin to decrease. This will result in a cooling of the melt pool and eventually resolidification into a solid layer. When the pool has completely resolidified, the process is over and the resolidified part will begin to cool to the ambient temperature.

This paper presents analysis of a one-dimensional model of the phase change undergone by the first layer of the SLS process on a cold powder bed. The true SLS process is, of course, a three-dimensional, multiple-layer process in which layer after layer of powder is added to the surface of the bed. A semi-infinite powder bed is assumed in this model, as in Zhang and Faghri [11], however, an analysis of a finite thickness powder bed with constant heat flux may be found in Chen and Zhang [12]. It is assumed that the liquid phase is incompressible and the melting point of the low melting point powder is not affected by changes in pressure. The radiation and convection from the liquid surface are neglected so that the excess heat of the liquid must be dissipated in the form of conduction into the powder bed in order for the melt pool to resolidify.

2.1. Governing equations

2.1.1. Preheating stage

During preheating the heat transfer in the powder bed can be described as a pure conduction problem. The heat conduction equation in the powder bed is

$$\frac{\partial T_s}{\partial t} = \alpha_s \frac{\partial^2 T_s}{\partial z^2}, \quad z > 0, \ -\infty < t < t_m \tag{2}$$

subject to the boundary conditions

$$T_s \to T_i, \quad z \to \infty, \ t > -\infty \tag{3}$$

$$T_s = T_i, \quad z \geqslant 0, \ t \to -\infty \tag{4}$$

The heat flux at the surface is governed by

$$-k_s \frac{\partial T_s}{\partial z} = q''(t), \quad z = 0, \ -\infty < t < t_m \tag{5}$$

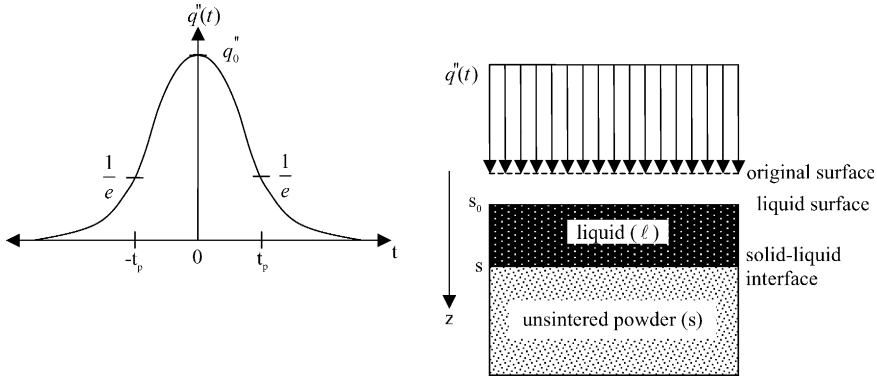

Fig. 1. The physical model.

where k_s is the effective conductivity of the unsintered powder bed and is related to the conductivities of the metal powder particles and the interstitial gas, k_p and k_g, as well as porosity, ε_s [13].

2.1.2. Melting with shrinkage stage

After melting has begun, $t \geqslant t_m$, the governing equation in the liquid phase is

$$\alpha_l \frac{\partial^2 T_l}{\partial z^2} = \frac{\partial T_l}{\partial t} + w\frac{\partial T_l}{\partial z}, \quad s_0 < z < s(t), \ t_m < t < t_{sol} \tag{6}$$

where t_{sol} is the time at which melting ends and solidification begins, and w is the velocity in the liquid induced by the shrinkage of the powder bed, which plays an important role on heat transfer in the liquid region as demonstrated by an order of magnitude analysis in Ref. [11]. Eq. (6) is subject to the following boundary condition

$$-k_l \frac{\partial T_l}{\partial z} = q''(t), \quad z = s_0, \ t_m < t < t_{sol} \tag{7}$$

The conductivity of the liquid melt pool, k_l, is obtained by

$$k_l = (1 - \varepsilon_l)k_p \tag{8}$$

Since the liquid is incompressible, the shrinkage velocity can be expressed by

$$w = \frac{ds_0}{dt}, \quad s_0 < z < s(t), \ t_m < t < t_{sol} \tag{9}$$

The governing equation for the solid phase (loose powder) after melting begins is

$$\frac{\partial T_s}{\partial t} = \alpha_s \frac{\partial^2 T_s}{\partial z^2}, \quad s(t) < z, \ t_m < t < t_{sol} \tag{10}$$

At the solid–liquid interface the temperature is

$$T_l(z,t) = T_s(z,t) = T_m, \quad z = s(t), \ t_m < t < t_{sol} \tag{11}$$

and the energy balance at the interface can be expressed as

$$k_s \frac{\partial T_s}{\partial z} - k_l \frac{\partial T_l}{\partial z} = (1 - \varepsilon_s)\phi\rho_L h_{sl}\frac{ds}{dt}, \quad z = s(t), \ t_m < t < t_{sol} \tag{12}$$

Based on the conservation of mass at the solid–liquid interface the shrinkage velocity, w, and the solid–liquid interface velocity, ds/dt, have the following relationship [11]

$$w = \frac{\varepsilon_s - \varepsilon_l}{1 - \varepsilon_l}\frac{ds}{dt} \tag{13}$$

2.1.3. Resolidification stage

As the heat flux at the surface of the powder bed decreases, heating of the powder bed will decrease and melting will begin to slow down and eventually stop. The point in time at which melting of the powder bed stops is also the point at which solidification begins, t_{sol}. At the time t_{sol} the shrinkage reaches its maximum value and thus the location of the surface of the powder bed is unchanged during the solidification time period meaning that s_0 = const. and $w = 0$.

Taking these two factors into consideration the governing equations after solidification begins are

$$\frac{\partial T_l}{\partial t} = \alpha_l \frac{\partial^2 T_l}{\partial z^2}, \quad s_0 > z > s(t), \ t > t_{sol} \tag{14}$$

$$-k_l \frac{\partial T_l}{\partial z} = q''(t), \quad z = s_0, \ t > t_{sol} \tag{15}$$

$$\frac{\partial T_s}{\partial t} = \alpha_s \frac{\partial^2 T_s}{\partial z^2}, \quad z > s(t = t_{sol}), \ t > t_{sol} \tag{16}$$

$$\frac{\partial T_r}{\partial t} = \alpha_r \frac{\partial^2 T_r}{\partial z^2}, \quad s(t) < z < s(t = t_{sol}), \ t > t_{sol} \tag{17}$$

$$T_l(z,t) = T_r(z,t) = T_m, \quad z = s(t), \ t > t_{sol} \tag{18}$$

$$k_r \frac{\partial T_r}{\partial z} - k_l \frac{\partial T_l}{\partial z} = (1 - \varepsilon_l)\phi\rho_L h_{sl}\frac{ds}{dt}, \quad z = s(t), \ t > t_{sol} \tag{19}$$

$$T_r(z,t) = T_s(z,t), \quad z = s(t = t_{sol}), \ t > t_{sol} \tag{20}$$

$$k_r \frac{\partial T_r}{\partial z} = k_s \frac{\partial T_s}{\partial z}, \quad z = s(t = t_{sol}), \ t > t_{sol} \tag{21}$$

$$\frac{\partial T_r}{\partial t} = \frac{\partial T_s}{\partial t}, \quad z = s(t = t_{sol}), \ t > t_{sol} \tag{22}$$

where the subscript r denotes the resolidified part, which is simply the solidified liquid phase. It is assumed that the properties of the resolidified region are the same as that of the liquid region (e.g., $k_r = k_l$).

2.2. Nondimensional governing equations

By defining the following dimensionless variables

$$\tau = \frac{t}{t_p}, \quad \tau_{sol} = \frac{t_{sol}}{t_p}, \quad \tau_m = \frac{t_m}{t_p}, \quad Z = \frac{z}{\sqrt{\alpha_p t_p}},$$
$$S = \frac{s}{\sqrt{\alpha_p t_p}}, \quad S_0 = \frac{s_0}{\sqrt{\alpha_p t_p}}, \quad W = \frac{t_p w}{\sqrt{\alpha_p t_p}},$$
$$K_g = \frac{k_g}{k_p}, \quad K_s = \frac{k_s}{k_p(1 - \varepsilon_s)}, \quad \bar{\alpha}_s = \frac{\alpha_s}{\alpha_p},$$
$$Ste = q_0''\frac{\sqrt{\alpha_p t_p}}{\alpha_p \phi h_{sl}\rho_L}, \quad \theta = \frac{(\rho c_p)_p}{\phi h_{sl}\rho_L}(T - T_m),$$
$$Sc = \frac{(\rho c_p)_p}{\phi h_{sl}\rho_L}(T_m - T_i) \tag{23}$$

the following dimensionless governing equations will be obtained.

2.2.1. Preheating stage

$$\frac{\partial\theta_s}{\partial\tau}=\bar{\alpha}_s\frac{\partial^2\theta_s}{\partial Z^2},\quad Z>0,\ -\infty<\tau<\tau_m \tag{24}$$

$$\frac{\partial\theta_s}{\partial Z}=-\frac{Ste\cdot e^{-\tau^2}}{K_s(1-\varepsilon_s)},\quad Z=0,\ -\infty<\tau<\tau_m \tag{25}$$

$$\theta_s=-Sc,\quad Z\geqslant 0,\ \tau=-\infty \tag{26}$$

$$\theta_s\to -Sc,\quad Z\to\infty,\ \tau>-\infty \tag{27}$$

2.2.2. Melting with shrinkage stage

$$\frac{\partial\theta_l}{\partial\tau}+W\frac{\partial\theta_l}{\partial Z}=\frac{\partial^2\theta_l}{\partial Z^2},\quad S_0<Z<S,\ \tau_m<\tau<\tau_{sol} \tag{28}$$

$$W=\frac{dS_0}{d\tau},\quad Z=S_0,\ \tau_m<\tau<\tau_{sol} \tag{29}$$

$$\frac{\partial\theta_l}{\partial Z}=-\frac{Ste\cdot e^{-\tau^2}}{(1-\varepsilon_l)},\quad Z=S_0,\ \tau_m<\tau<\tau_{sol} \tag{30}$$

$$\frac{\partial\theta_s}{\partial\tau}=\bar{\alpha}_s\frac{\partial^2\theta_s}{\partial Z^2},\quad S(\tau)<Z<\infty,\ \tau_m<\tau<\tau_{sol} \tag{31}$$

$$\theta_l(Z,\tau)=\theta_s(Z,\tau)=0,\quad Z=S(\tau),\ \tau_m<\tau<\tau_{sol} \tag{32}$$

$$K_s\frac{\partial\theta_s}{\partial Z}-\frac{1-\varepsilon_l}{1-\varepsilon_s}\frac{\partial\theta_l}{\partial Z}=\frac{dS}{d\tau},\quad Z=S(\tau),\ \tau_m<\tau<\tau_{sol} \tag{33}$$

$$W=\frac{\varepsilon_s-\varepsilon_l}{1-\varepsilon_l}\frac{dS}{d\tau},\quad S_0<Z<S(\tau),\ \tau_m<\tau<\tau_{sol} \tag{34}$$

2.2.3. Solidification stage

$$\frac{\partial\theta_l}{\partial\tau}=\frac{\partial^2\theta_l}{\partial Z^2},\quad S_0<Z<S(\tau),\ \tau>\tau_{sol} \tag{35}$$

$$\frac{\partial\theta_l}{\partial Z}=-\frac{Ste\cdot e^{-\tau^2}}{1-\varepsilon_l},\quad Z=S_0,\ \tau>\tau_{sol} \tag{36}$$

$$\frac{\partial\theta_s}{\partial\tau}=\bar{\alpha}_s\frac{\partial^2\theta_s}{\partial Z^2},\quad S(\tau=\tau_{sol})<Z,\ \tau>\tau_{sol} \tag{37}$$

$$\frac{\partial\theta_r}{\partial\tau}=\frac{\partial^2\theta_r}{\partial Z^2},\quad S(\tau)<Z<S(\tau=\tau_{sol}),\ \tau>\tau_{sol} \tag{38}$$

$$\theta_l(Z,\tau)=\theta_r(Z,\tau)=0,\quad Z=S(\tau),\ \tau>\tau_{sol} \tag{39}$$

$$\frac{\partial\theta_r}{\partial Z}-\frac{\partial\theta_l}{\partial Z}=\frac{dS}{d\tau},\quad Z=S(\tau),\ \tau>\tau_{sol} \tag{40}$$

$$\theta_r(Z,\tau)=\theta_s(Z,\tau),\quad Z=S(\tau=\tau_{sol}),\ \tau>\tau_{sol} \tag{41}$$

$$\frac{\partial\theta_r}{\partial Z}=K_s\frac{1-\varepsilon_s}{1-\varepsilon_l}\frac{\partial\theta_s}{\partial Z},\quad Z=S(\tau=\tau_{sol}),\ \tau>\tau_{sol} \tag{42}$$

$$\frac{\partial\theta_r}{\partial\tau}=\frac{\partial\theta_s}{\partial\tau},\quad Z=S(\tau=\tau_{sol}),\ \tau>\tau_{sol} \tag{43}$$

The solutions of all three stages will be obtained by using the integral approximate method and assuming second degree polynomial temperature profiles.

3. The integral approximate solution

When the surface of the powder bed is exposed to heat flux the heat will penetrate the surface and begin to conduct downward. The depth to which the heat flux has penetrated is called the thermal penetration depth, δ, beyond which the temperature is equal to the initial powder bed temperature. Therefore, the following two dimensionless boundary conditions at the dimensionless thermal penetration depth, $\Delta=\delta/\sqrt{\alpha_p t_p}$, are valid:

$$\theta_s(Z)=-Sc,\quad Z\geqslant\Delta(\tau),\ \tau>-\infty \tag{44}$$

$$\frac{\partial\theta_s}{\partial Z}=0,\quad Z\geqslant\Delta(\tau),\ \tau>-\infty \tag{45}$$

3.1. Solution for the preheating stage

Integrating both sides of Eq. (24) with respect to Z in the interval of $(0,\Delta)$ and applying the Leibniz's Rule yields

$$\frac{1}{\bar{\alpha}_s}\left[\frac{d}{d\tau}\int_0^{\Delta}\theta_s\,dZ-\theta_s(\Delta)\frac{d\Delta}{d\tau}\right]=\left.\frac{\partial\theta_s}{\partial Z}\right|_0^{\Delta} \tag{46}$$

Substituting Eqs. (25), (44) and (45) into Eq. (46), the integral equation becomes

$$\frac{1}{\bar{\alpha}_s}\left[\frac{d}{d\tau}\int_0^{\Delta}\theta_s\,dZ+Sc\frac{d\Delta}{d\tau}\right]=\frac{Ste}{K_s(1-\varepsilon_s)}e^{-\tau^2} \tag{47}$$

Assuming that the temperature distribution is a second degree polynomial function and solving the unknown constants using the boundary conditions of Eqs. (25), (44), and (45), the temperature distribution in the thermal penetration depth becomes

$$\theta_s(Z,\tau)=-Sc+\frac{Ste}{2\Delta K_s(1-\varepsilon_s)}e^{-\tau^2}(\Delta-Z)^2,\quad \tau<\tau_m \tag{48}$$

Substituting Eq. (48) into Eq. (47) yields

$$\frac{d}{d\tau}\left[e^{-\tau^2}\Delta^2\right]=6\bar{\alpha}_s e^{-\tau^2} \tag{49}$$

which is subjected to the following initial condition

$$\Delta=0,\quad \tau=-\infty \tag{50}$$

Integrating Eq. (49) in the interval $(-\infty,\tau)$, one obtains

$$e^{-\tau^2}\Delta^2 = 6\bar{\alpha}_s\int_{-\infty}^{\tau} e^{-\tau^2}\,d\tau \tag{51}$$

The thermal penetration depth in the powder bed can be expressed in terms of the error function, i.e.,

$$\Delta = \sqrt{3\sqrt{\pi}\bar{\alpha}_s e^{\tau^2}[1+\mathrm{erf}(\tau)]}, \quad \tau < \tau_m \tag{52}$$

When melting begins at time $\tau = \tau_m$ the temperature of the powder bed surface will be equal to the melting point of the low melting point powder, $\theta_s = 0$, i.e.,

$$\theta_s(0,\tau_m) = 0 = -Sc + \frac{Ste\cdot e^{-\tau_m^2}\cdot\Delta_m}{2K_s(1-\varepsilon_s)} \tag{53}$$

The thermal penetration depth at the end of preheating can be obtained from Eq. (52)

$$\Delta_m = \sqrt{3\sqrt{\pi}\bar{\alpha}_s e^{\tau_m^2}[1+\mathrm{erf}(\tau_m)]} \tag{54}$$

Eqs. (53) and (54) give two equations for two unknowns which can be solved to find

$$\tau_m = \pm\sqrt{\ln\left[\frac{3\sqrt{\pi}\bar{\alpha}_s Ste^2[1+\mathrm{erf}(\tau_m)]}{4Sc^2K_s^2(1-\varepsilon_s)^2}\right]} \tag{55}$$

Because laser intensity is at its highest when time $\tau = 0$, the time at which melting begins will be the negative value of Eq. (55). Due to the error function expression τ_m must be solved for in an iterative fashion.

3.2. Solution for the melting stage

3.2.1. Loose powder region

Although preheating ends when the temperature at the surface of the powder bed meets the melting point of the low melting point powder, the solution for the loose powder is still needed in the region from the solid–liquid interface to the thermal penetration depth. The following procedure is nearly identical to the preheating solution, the principal change being the limits of integration.

Integrating both sides of Eq. (31) with respect to Z in the interval of (S,Δ) and applying Leibniz's Rule yields

$$\frac{1}{\bar{\alpha}_s}\left[\frac{d}{d\tau}\int_S^{\Delta}\theta_s\,dZ - \theta_s(\Delta)\frac{d\Delta}{d\tau} + \theta_s(S)\frac{dS}{d\tau}\right] = \left.\frac{\partial\theta_s}{\partial Z}\right|_S^{\Delta} \tag{56}$$

Substituting the boundary conditions given by Eqs. (32), (44) and (45) into Eq. (56) gives

$$\frac{-1}{\bar{\alpha}_s}\left[\frac{d}{d\tau}\int_S^{\Delta}\theta_s\,dZ + Sc\frac{d\Delta}{d\tau}\right] = \left.\frac{\partial\theta_s}{\partial Z}\right|_S \tag{57}$$

Assuming that the temperature distribution is a second degree polynomial function and solving for the unknown constants using the boundary conditions given by Eqs. (32), (44) and (45) the assumed nondimensional temperature profile is

$$\theta_s(Z,\tau) = Sc\left[\left(\frac{\Delta-Z}{\Delta-S}\right)^2 - 1\right] \tag{58}$$

Substituting Eq. (58) into Eq. (57) yields

$$\frac{6\bar{\alpha}_s}{\Delta-S} = \frac{d\Delta}{d\tau} + 2\frac{dS}{d\tau} \tag{59}$$

which describes the relationship between the location of the solid–liquid interface and the thermal penetration depth. It is subject to the initial conditions

$$\Delta = \Delta_m, \quad \tau = \tau_m \tag{60}$$

$$S = 0, \quad \tau = \tau_m \tag{61}$$

3.2.2. Liquid region

Integrating Eq. (28) in the interval (S_0,S) and applying Leibniz's Rule gives

$$\left.\frac{\partial\theta_l}{\partial Z}\right|_S - \left.\frac{\partial\theta_l}{\partial Z}\right|_{S_0} = \frac{d}{d\tau}\int_{S_0}^{S}\theta_l\partial Z + \theta_l(S_0)\frac{dS_0}{d\tau} - \theta_l(S)\frac{dS}{d\tau} + W[\theta_l(S)-\theta_l(S_0)] \tag{62}$$

Applying the boundary conditions given from Eqs. (30) and (32) and recalling Eq. (29), (62) is reduced to

$$\frac{d}{d\tau}\int_{S_0}^{S}\theta_l\,dZ - \frac{Ste}{1-\varepsilon_l}e^{-\tau^2} = \left.\frac{\partial\theta_l}{\partial Z}\right|_S \tag{63}$$

At this point a second degree polynomial temperature distribution of the form

$$\theta_l(Z,\tau) = A + B\left(\frac{Z-S}{S}\right) + C\left(\frac{Z-S}{S}\right)^2 \tag{64}$$

will be assumed in the liquid. The boundary conditions of Eqs. (30) and (32) will not be enough to solve for the three undetermined coefficients of Eq. (64) so another boundary condition must be established. The additional boundary condition is found by differentiating Eq. (32)

$$d\theta_l = \frac{\partial\theta_l}{\partial Z}dZ + \frac{\partial\theta_l}{\partial\tau}d\tau = 0, \quad Z = S(\tau), \ \tau_m > \tau > \tau_{sol} \tag{65}$$

which can be rearranged to yield

$$\frac{\partial\theta_l}{\partial Z}\frac{dS}{d\tau} + \frac{\partial\theta_l}{\partial\tau} = 0, \quad Z = S(\tau), \ \tau > \tau_m \tag{66}$$

Substituting Eqs. (28) and (33) into Eq. (66), one obtains

$$K_s\left.\frac{\partial\theta_s}{\partial Z}\right|_S\left.\frac{\partial\theta_l}{\partial Z}\right|_S - \frac{1-\varepsilon_l}{1-\varepsilon_s}\left(\left.\frac{\partial\theta_l}{\partial Z}\right|_S\right)^2 + \left.\frac{\partial^2\theta_l}{\partial Z^2}\right|_S - W\left.\frac{\partial\theta_l}{\partial Z}\right|_S = 0 \tag{67}$$

Eqs. (33) and (34), and the partial derivative of Eq. (58) can be used to simplify Eq. (67) and give us the final boundary condition of

$$-\left(\frac{\partial\theta_l}{\partial Z}\bigg|_S\right)^2-\frac{1-\varepsilon_s}{1-\varepsilon_l}\frac{2ScK_s}{\Delta-S}\frac{\partial\theta_l}{\partial Z}\bigg|_S+\frac{\partial^2\theta_l}{\partial Z^2}\bigg|_S=0 \tag{68}$$

The boundary conditions of Eqs. (30), (32), and (68) will be used to solve for the coefficients of the assumed liquid temperature profile in Eq. (64). Upon elimination of coefficient A and B using Eqs. (30) and (32), the temperature profile in the liquid phase becomes

$$\theta_l(Z,\tau)=\left[\frac{-S\cdot Ste}{1-\varepsilon_l}e^{-\tau^2}+2C\frac{1-\varepsilon_s}{1-\varepsilon_l}\right]\left(\frac{Z-S}{S}\right)+C\left(\frac{Z-S}{S}\right)^2 \tag{69}$$

Substituting Eqs. (58) and (69) into Eq. (68), an algebraic equation of C is obtained.

$$\begin{aligned}&\left[-4\frac{(1-\varepsilon_s)^2}{(1-\varepsilon_l)^2}\right]C^2\\&+\left[2+4Ste\frac{1-\varepsilon_s}{(1-\varepsilon_l)^2}e^{-\tau^2}S+\frac{-4ScK_s}{(\Delta-S)}\frac{(1-\varepsilon_s)^2}{(1-\varepsilon_l)^2}S\right]C\\&+\left[\frac{-Ste^2}{(1-\varepsilon_l)^2}e^{-2\tau^2}S^2+Ste\cdot e^{-\tau^2}\frac{2ScK_s}{(\Delta-S)}\frac{(1-\varepsilon_s)}{(1-\varepsilon_l)^2}S^2\right]\\&=0\end{aligned} \tag{70}$$

where the relation $S_0-S=-S(1-\varepsilon_s)/(1-\varepsilon_l)$, obtained by combining Eqs. (29) and (34) was used to simplify the equations.

Since the assumed temperature distributions for both phases are known, the next task is to find the location of the solid–liquid interface, S, and the thermal penetration depth, Δ. Substituting Eqs. (57) and (63) into Eq. (33) gives

$$\begin{aligned}&\frac{-K_s}{\bar{\alpha}_s}\left[\frac{d}{d\tau}\int_S^{\Delta}\theta_s\,dZ+Sc\frac{d\Delta}{d\tau}\right]\\&-\frac{1-\varepsilon_l}{1-\varepsilon_s}\left[\frac{d}{d\tau}\int_{S_0}^{S}\theta_l\,dZ-\frac{Ste}{1-\varepsilon_l}e^{-\tau^2}\right]=\frac{dS}{d\tau},\\&Z=S(\tau),\quad\tau>\tau_m\end{aligned} \tag{71}$$

which can be integrated with respect to τ over the interval (τ_m,τ) and simplified to yield

$$\begin{aligned}S=&\frac{-K_s}{\bar{\alpha}_s}\left[\int_S^{\Delta}\theta_s\,dZ-\int_0^{\Delta_m}\theta_s\,dZ+Sc(\Delta-\Delta_m)\right]\\&-\frac{1-\varepsilon_l}{1-\varepsilon_s}\int_{S_0}^{S}\theta_l\,dZ+\frac{Ste\sqrt{\pi}}{2(1-\varepsilon_s)}[\mathrm{erf}(\tau)-\mathrm{erf}(\tau_m)]\end{aligned} \tag{72}$$

If the integrals in Eq. (72) are evaluated and then terms are collected for S, a second order polynomial equation of S is obtained.

$$\begin{aligned}&\left[-\frac{1}{2}Ste\frac{1-\varepsilon_s}{(1-\varepsilon_l)^2}e^{-\tau^2}\right]S^2\\&+\left[-1-\frac{2}{3}\frac{ScK_s}{\bar{\alpha}_s}+\frac{2}{3}C\left(\frac{1-\varepsilon_s}{1-\varepsilon_l}\right)^2\right]S\\&+\left[-\frac{1}{3}\frac{ScK_s}{\bar{\alpha}_s}(\Delta-\Delta_m)+\frac{Ste\sqrt{\pi}}{2(1-\varepsilon_s)}[\mathrm{erf}(\tau)-\mathrm{erf}(\tau_m)]\right]\\&=0\end{aligned} \tag{73}$$

The roots of Eq. (73) will be the possible values of S, the location of the solid–liquid interface. To find Δ, the location of the thermal penetration depth, integrate both sides of Eq. (59) with respect to τ over the interval (τ_m,τ) to yield

$$\Delta=\Delta_m-2S+\int_{\tau_m}^{\tau}\frac{6\bar{\alpha}_s}{\Delta-S}\,d\tau \tag{74}$$

By solving Eqs. (74) and (73) the locations of the solid–liquid interface and the thermal penetration depth in the powder bed will be found. The integral on the right side of Eq. (74) must be evaluated using numerical integration.

3.3. Solution for the solidification stage

As the heat flux at the surface of the powder bed decreases melting will slow down and eventually stop. When melting stops the motion of the solid–liquid interface will reverse direction and begin to move back toward the surface of the powder bed as the melt pool solidifies. Since melting has stopped there is no longer a density change in the powder bed and shrinkage of the powder bed has ceased. The location of the liquid surface during the solidification period is fixed, meaning that $S_0=$ const. and $W=0$. These factors will be taken into account during the solution of the solidification period.

3.3.1. Loose powder region

Integrating both sides of Eq. (37) in the interval (S_{sol},Δ) and applying the boundary condition of Eq. (45) gives the integral equation in the loose powder

$$\frac{-1}{\bar{\alpha}_s}\left[\frac{d}{d\tau}\int_{S_{sol}}^{\Delta}\theta_s\,dZ+Sc\frac{d\Delta}{d\tau}\right]=\frac{\partial\theta_s}{\partial Z}\bigg|_{S_{sol}} \tag{75}$$

where S_{sol} is the location of the solid–liquid interface at the time $\tau=\tau_{sol}$.

Assuming a second degree polynomial and applying the boundary conditions of Eqs. (44) and (45) to

eliminate two of the three coefficients, the temperature in the solid, unsintered powder then becomes

$$\theta_s(Z,\tau) = A_s + \frac{-2(A_s+Sc)}{\Delta - S_{sol}}(Z - S_{sol}) + \frac{A_s+Sc}{(\Delta - S_{sol})^2}(Z-S_{sol})^2, \quad S_{sol} < Z < \Delta(\tau) \tag{76}$$

The thermal penetration depth can be found by integrating Eq. (75) once from τ_{sol} to τ. Using the temperature distribution of Eq. (76) to evaluate the integral of θ_s from S_{sol} to Δ one obtains

$$\Delta(\tau) = \frac{6\bar{\alpha}_s}{A_s+Sc}\int_{\tau_{sol}}^{\tau}\frac{A_s+Sc}{\Delta - S_{sol}}\,d\tau + \frac{A_s S_{sol} + Sc\,\Delta_{sol}}{A_s+Sc}, \quad \tau_{sol} < \tau < \tau_{final} \tag{77}$$

3.3.2. Resolidified region

The resolidified region is simply the portion of the melt pool that has resolidified. By integrating Eq. (38) once and applying the boundary conditions of Eqs. (39) and S_{sol} = const. the integral energy equation for the resolidified region becomes

$$\frac{d}{d\tau}\int_S^{S_{sol}}\theta_r\,dZ = \left.\frac{\partial\theta_r}{\partial Z}\right|_{S_{sol}} - \left.\frac{\partial\theta_r}{\partial Z}\right|_S, \quad S(\tau) < Z < S_{sol} \tag{78}$$

By assuming a second degree polynomial for the temperature distribution in the resolidified part and applying the boundary conditions of Eqs. (39), (41), and (42), the temperature profile in the resolidified region becomes

$$\theta_r(Z) = \left[\frac{2A_s}{S_{sol}-S} + \frac{2K_s(A_s+Sc)}{\Delta - S_{sol}}\frac{1-\varepsilon_s}{1-\varepsilon_l}\right](Z-S) + \left[\frac{-A_s}{(S_{sol}-S)^2} - \frac{2K_s(A_s+Sc)}{(\Delta - S_{sol})(S_{sol}-S)}\frac{1-\varepsilon_s}{1-\varepsilon_l}\right] \times (Z-S)^2, \quad S(\tau) < Z < S_{sol} \tag{79}$$

where A_s is still unknown at this point.

To determine the coefficient A_s, the temperature at $Z = S_{sol}$, a combination of Eqs. (37), (38), and (43) are used and the result is

$$A_s = \frac{2ScK_s(1-\varepsilon_s)(S_{sol}-S)(\Delta - S_{sol}) + \bar{\alpha}_s Sc(S_{sol}-S)^2(1-\varepsilon_l)}{-(\Delta - S_{sol})^2(1-\varepsilon_l) - 2K_s(1-\varepsilon_s)(S_{sol}-S)(\Delta - S_{sol}) - \bar{\alpha}_s(S_{sol}-S)^2(1-\varepsilon_l)} \tag{80}$$

3.3.3. Liquid region

The solution for the liquid region of the solidification stage can be obtained in a manor similar to the solution for the liquid region of the melting stage. Beginning with Eq. (35) integrate both sides, use Leibniz's Rule, and apply the boundary conditions given by Eqs. (36) and (39) to get the integral energy equation in the melt pool

$$\frac{\partial}{\partial\tau}\int_{S_0}^{S}\theta_l\,dZ - \frac{Ste}{1-\varepsilon_l}e^{-\tau^2} = \left.\frac{\partial\theta_l}{\partial Z}\right|_S \tag{81}$$

Assuming that the temperature distribution in the liquid has the form of a second degree polynomial and applying the boundary conditions of Eqs. (36) and (39) to eliminate two of the three coefficients, the temperature distribution in the liquid becomes

$$\theta_l(Z,\tau) = \left[-\frac{Ste}{1-\varepsilon_l}e^{-\tau^2}S - \frac{2C_1}{S}(S_0 - S)\right]\left(\frac{Z-S}{S}\right) + C_1\left(\frac{Z-S}{S}\right)^2 \tag{82}$$

where the coefficient C_1 will be found using a procedure similar to the one used to find C_1 in the melting stage. The result of this process is

$$\left[\frac{-4(S-S_0)^2}{S^2}\right]C_1^2 + \left[2 + \frac{4Ste}{1-\varepsilon_l}e^{-\tau^2}(S-S_0) + 4(A_s+Sc)K_s\frac{1-\varepsilon_s}{1-\varepsilon_l}\frac{S_0-S}{S_{sol}-\Delta} - 4A_s\frac{S_0-S}{S_{sol}-S}\right]C_1 + \left[\frac{-Ste^2}{(1-\varepsilon_l)^2}e^{-2\tau^2}S^2 - \frac{2A_s}{1-\varepsilon_l}\frac{Ste\cdot e^{-\tau^2}}{S_{sol}-S}S^2 + \frac{2K_s(Sc+A_s)}{S_{sol}-\Delta}Ste\cdot e^{-\tau^2}S^2\frac{1-\varepsilon_s}{(1-\varepsilon_l)^2}\right] = 0 \tag{83}$$

which is different from Eq. (70) because S_0 = const. in the solidification stage. The two roots of this polynomial can found, each of which will correspond to a possible value of C_1.

In order to find how S changes with time the integral energy equations, Eqs. (78) and (81), must be substituted into the energy balance equation at the resolidified part-liquid pool interface, Eq. (40), to give

$$\frac{dS}{d\tau} = \left.\frac{\partial\theta_r}{\partial Z}\right|_{S_{sol}} - \frac{\partial}{\partial\tau}\int_S^{S_{sol}}\theta_r\,dZ - \frac{\partial}{\partial\tau}\int_{S_0}^{S}\theta_l\,dZ + \frac{Ste\cdot e^{-\tau^2}}{1-\varepsilon_l} \tag{84}$$

Recalling the assumed temperature profiles of Eqs. (79) and (82), Eq. (84) can be integrated from τ_{sol} to τ and terms of S collected to find the polynomial

$$\left[\frac{-Ste\cdot e^{-\tau^2}}{2(1-\varepsilon_l)}+\frac{1-\varepsilon_s}{1-\varepsilon_l}\frac{K_s(A_s+Sc)}{3(S_{sol}-\Delta)}\right]S^4+\left[-1+\frac{2}{3}(A_s+C_l)+\frac{Ste\cdot e^{-\tau^2}}{(1-\varepsilon_l)}S_0-\frac{2}{3}\frac{1-\varepsilon_s}{1-\varepsilon_l}\frac{K_s(A_s+Sc)}{(S_{sol}-\Delta)}S_{sol}\right]S^3+\left[-2K_s\frac{1-\varepsilon_s}{1-\varepsilon_l}\int_{\tau_{sol}}^{\tau}\frac{A_s+Sc}{\Delta-S_{sol}}\,d\tau-2C_lS_0+S_{sol}+\frac{2C_{l,sol}}{3S_{sol}^2}(S_0-S_{sol})^3-\frac{2}{3}A_sS_{sol}-\frac{Ste\cdot e^{-\tau^2}}{2(1-\varepsilon_l)}S_0^2+\frac{Ste\cdot e^{-\tau_{sol}^2}}{2(1-\varepsilon_l)}(S_0-S_{sol})^2+\frac{1}{3}\frac{1-\varepsilon_s}{1-\varepsilon_l}\frac{K_s(A_s+Sc)}{(S_{sol}-\Delta)}S_{sol}^2+\frac{Ste\sqrt{\pi}}{2(1-\varepsilon_l)}[\mathrm{erf}(\tau)-\mathrm{erf}(\tau_{sol})]\right]S^2+[2C_lS_0^2]S+\left[-\frac{2}{3}C_lS_0^3\right]=0 \tag{85}$$

one of the roots of which will be the location of the liquid-resolidified region interface. $C_{\ell,\ sol}$ is simply the value of C_l at the time $\tau=\tau_{sol}$ or

$$\left[\frac{-4(S_{sol}-S_0)^2}{S_{sol}^2}\right]C_{l,sol}^2+\left[2+\frac{4Ste\cdot e^{-\tau_{sol}^2}}{1-\varepsilon_l}(S_{sol}-S_0)+4ScK_s\frac{1-\varepsilon_s}{1-\varepsilon_l}\frac{S_0-S_{sol}}{S_{sol}-\Delta_{sol}}\right]C_{l,sol}+\left[\frac{-Ste^2\cdot e^{-2\tau_{sol}^2}}{(1-\varepsilon_l)^2}S_{sol}^2+S_{sol}^2Ste\cdot e^{-\tau_{sol}^2}\frac{1-\varepsilon_s}{(1-\varepsilon_l)^2}\frac{2ScK_s}{S_{sol}-\Delta_{sol}}\right]=0 \tag{86}$$

Now that all of the necessary components to describe the location of the solid–liquid interface, the location of the liquid surface, and the temperature distributions for each time period have been found a computer simulation can be developed to give the results of the model.

4. Results and discussion

The solutions of the preheating, melting, and resolidification stages have been derived in terms of nondimensional parameters. A computer program was written to simulate the results of the model and the nondimensional parameters were varied to investigate the impact they would have on the sintering process. In all of the following simulations the material properties of the low melting point powder are that of aluminum and the material properties of the high melting point powder are that of titanium. The most important processing parameter is Stefan number. It is proportional to $q_0''\sqrt{t_p}$ [see Eq. (23)] and it can be affected by a change in either laser power or laser pulse width. The range of the Stefan number used in this study is obtained by using a peak heat flux on the order of $2\times10^6\ \mathrm{W\ m^{-2}}$ and a laser pulse width of less than 0.50 s. The porosity of the liquid phase, ε_l, was assumed to be 10%, meaning that not all of the interstitial gas in the powder bed is driven out during the melting stage. The porosity of the unsintered powder, ε_s, was assumed to be 40%. The value of ϕ, the percentage of low melting point powder in the powder bed, was chosen to be 40%. Resulting values of the nondimensional parameters can be found in the captions of the following figures.

Fig. 2 shows the temperature profile within the powder bed at various times during a simulation for the baseline values of the dimensionless parameters. It shows an increase in temperature throughout the powder bed as the process continues. The line corresponding to $\tau=\tau_{peak}$ is the time at which the surface of the powder bed reaches its maximum temperature. Note that the temperature profile lines for $\tau\geqslant\tau_m$ do not extend all the way to $Z=0$ due to shrinkage of the powder bed. The progression of the thermal penetration depth during the duration of the process can also be seen in the figure.

Fig. 3 shows the change in temperature at the surface of the powder bed for different values of the Stefan number. The surface temperature increases as the heat flux increases, with the peak surface temperature occurring after $\tau=0$, the time at which maximum heat flux occurs. It can also be see in Fig. 3 that as the Stefan number increases the time at which melting begins decreases.

Fig. 4 shows the effect of the Stefan number, or the magnitude of the heat flux, on the locations of the solid–liquid interface, the liquid surface, and the thermal penetration depth. Obviously as the Stefan number increases the melt pool depth increases and the temperature of the melt pool surface increases, as evidenced by Fig. 3. A higher Stefan number will also result in more shrinkage, because more material will be melted, and a longer process time, because it will take longer for this increased quantity of melted powder to cool and resolidify.

Fig. 5 shows the location of the liquid surface and the solid–liquid interface for the same Stefan number but different subcooling parameters. For $Sc=4.0$ the laser beam pass makes a relatively shallow melt pool as compared to the hotter powder bed of $Sc=3.0$. For the subcooling parameter of $Sc=2.0$ the melt pool is very deep because the laser does not have to do nearly as much preheating. The higher the subcooling parameter, the greater the difference between the initial temperature of the powder bed and the melting point of the low melting point powder. Thus the higher the subcooling parameter the more heat flux is needed to melt the powder and the longer it takes for melting to begin, which is confirmed by Fig. 5.

Obviously a powder bed that is very porous will experience a greater amount of shrinkage due to melting than one that is less porous, however, Fig. 6 shows that a very porous powder bed will also have a deeper melt pool and

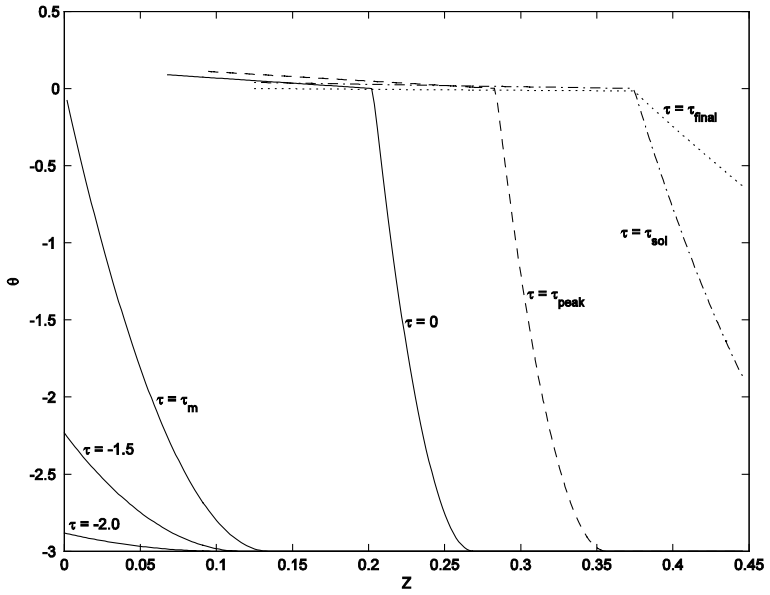

Fig. 2. The temperature profile within the powder bed at various times ($Ste = 0.6, Sc = 3.0, \varepsilon_s = 0.40, \varepsilon_l = 0.10, \phi = 0.40, \bar{\alpha}_s = 0.0081, K_s = 0.0081$).

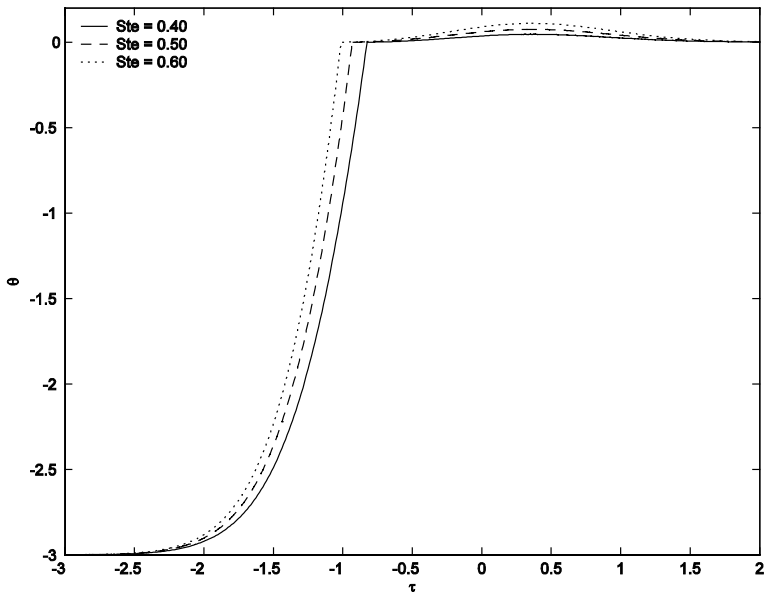

Fig. 3. The surface temperature of the powder bed for various values of the Stefan number ($Sc = 3.0, \varepsilon_s = 0.40, \varepsilon_l = 0.10, \phi = 0.40, \bar{\alpha}_s = 0.0081, K_s = 0.0081$).

a longer process time. This is because as the porosity of the metal powder increases the effective thermal conductivity of the powder bed decreases. A very porous powder bed will reach the end of the preheating period faster than a less porous one, and a greater volume of powder bed will be sintered, because the lower thermal conductivity will keep more of the heat flux at the surface of the powder bed, essentially not letting the heat flux penetrate the powder bed as quickly as a densely packed powder bed. This porosity will increase the process time significantly because in the model heat in the melt pool can only be lost via conduction of the heat deeper into the loose powder bed, not by radiation or convection at the surface.

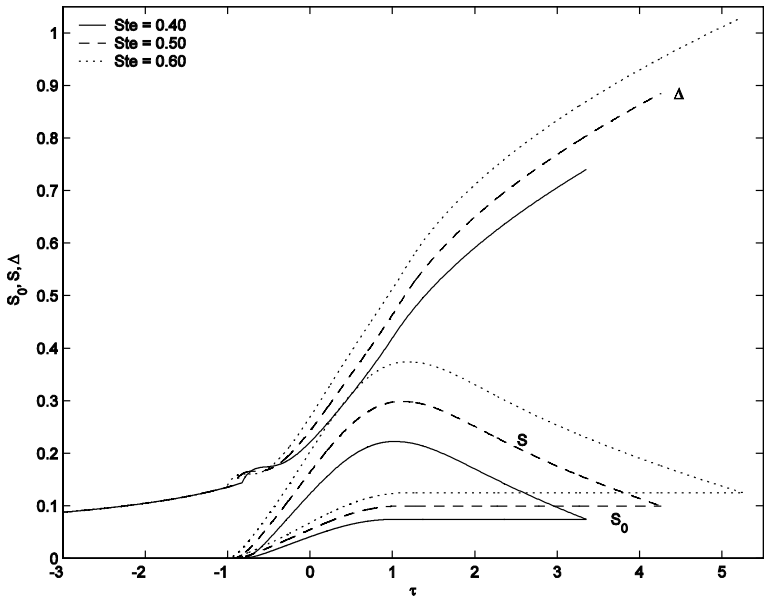

Fig. 4. The location of the liquid surface, the solid–liquid interface, and the thermal penetration depth for various of the Stefan number ($Sc = 3.0, \varepsilon_s = 0.40, \varepsilon_l = 0.10, \phi = 0.40, \bar{\alpha}_s = 0.0081, K_s = 0.0081$).

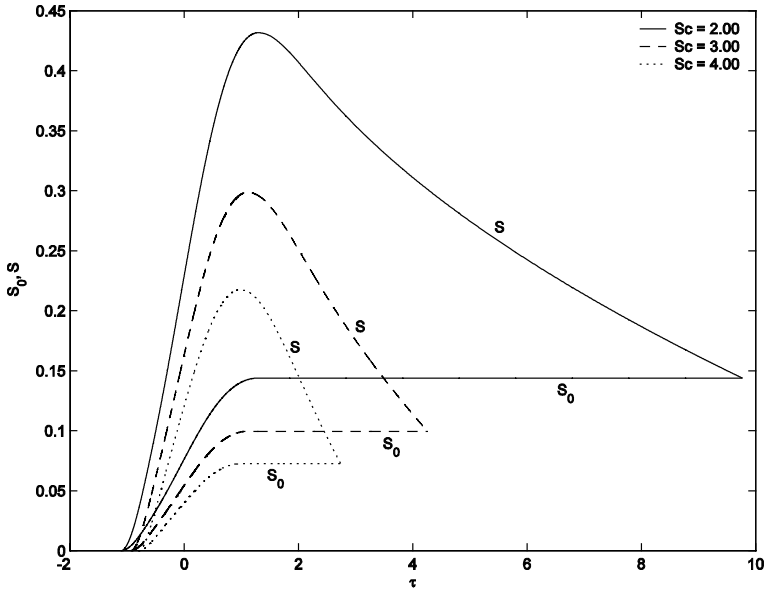

Fig. 5. The effect of the subcooling parameter on the location of the liquid surface and the solid–liquid interface ($Ste = 0.5, \varepsilon_s = 0.40$, $\varepsilon_l = 0.10, \phi = 0.40, \bar{\alpha}_s = 0.0081, K_s = 0.0081$).

Fig. 7 shows the effect of a change in the fraction of low melting point powder in the powder bed. The figure shows that as the fraction of low melting point powder in the powder bed increases the process time increases and the amount of melted material increases. This makes sense because if there is more low melting point powder in the powder bed then more material will be melted by the applied heat flux. More melted material means that more latent heat must be dissipated into the unsintered powder after the temporal Gaussian heat flux has decreased, hence an increase in process time.

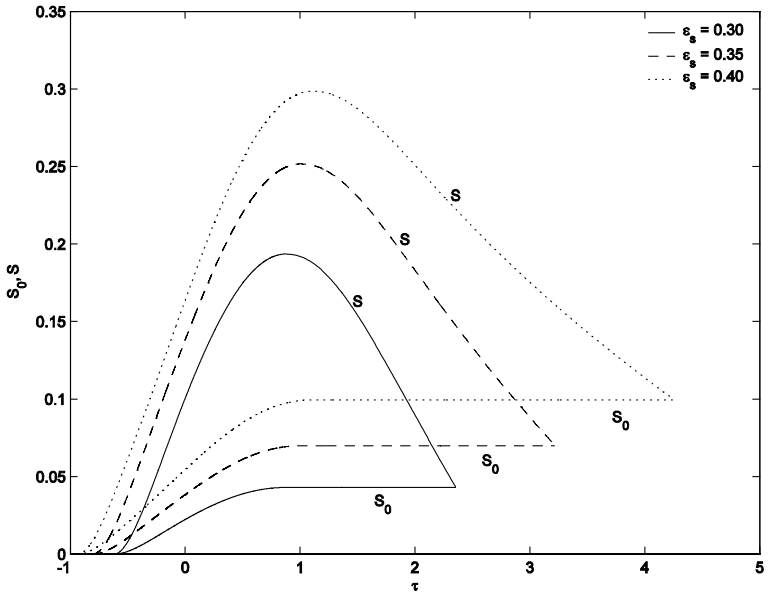

Fig. 6. The effect of the porosity of the unsintered powder on the location of the liquid surface and the solid liquid interface (Ste = 0.5, Sc = 3.0, ε_l = 0.10, ϕ = 0.40).

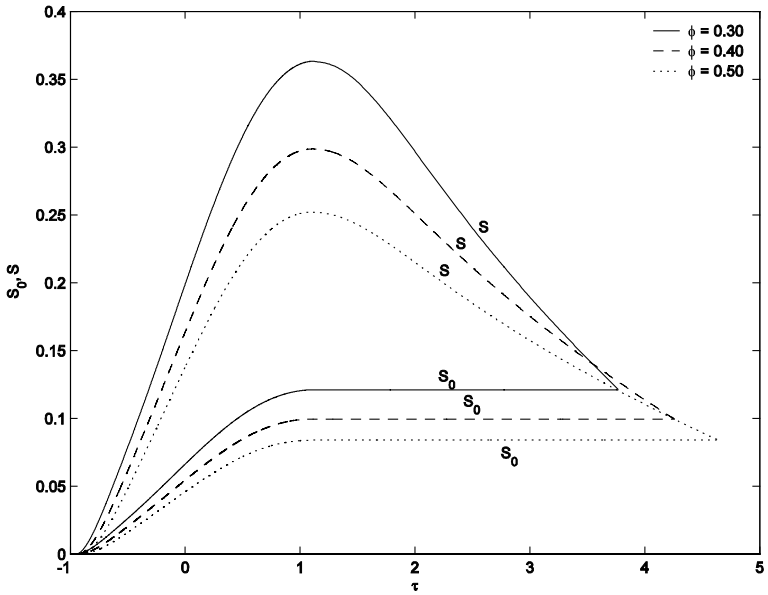

Fig. 7. The effect of the fraction of low melting point powder on the location of the liquid surface and the solid–liquid interface (ε_s = 0.40, ε_l = 0.10).

5. Conclusion

Melting and solidification in a subcooled powder bed with temporal Gaussian heat flux was investigated analytically. It is clear that all process parameters have effects on the results of the SLS process but through nondimensionalization the number of independent parameters can be significantly reduced. As the Stefan number is increased the melt pool depth is also increased as well as the temperature of the melt pool surface and the overall process time. As subcooling of the powder bed increases more heat flux is needed to melt the powder, and thus the melt pool is shallower. It was found that a very porous powder bed will reach the end of

the preheating period faster than a less porous one, a greater amount of material will be sintered, and the total process time will also increase. An increase in the fraction of low melting point powder will mainly increase the process time. The physical model and results of this investigation pave the way for further modeling of SLS processes with a pulsed laser.

Acknowledgement

Support for this work by the office of Naval Research (ONR) under grant number 00014-02-1-0356 is gratefully acknowledged.

References

[1] M. Agarwala, D. Bourell, J. Beaman, H. Marcus, J. Barlow, Direct selective laser sintering of metals, Rapid Prototyping J. 1 (1) (1995) 26–36.
[2] S. Das, J. Beaman, M. Wohlert, D. Bourell, Direct laser freeform fabrication of high performance metal components, Rapid Prototyping J. 4 (3) (1998) 112–117.
[3] P. Fischer, V. Romano, H.P. Weber, N.P. Karapatis, E. Boillat, R. Glardon, Sintering of commercially pure titanium powder with a Nd:YAG laser source, Acta Mater. 51 (6) (2003) 1651–1662.
[4] F. Abe, E. Costa Santos, Y. Kitamura, K. Osakada, M. Shiomi, Influence of forming conditions on the titanium model in rapid prototyping with the selective laser melting process, Proc. Inst. Mech. Engrs. Part C—J. Mech. Eng. Sci. 217 (1) (2003) 119–126.
[5] N.K. Tolochko, S.E. Mozzharov, I.A. Yadroitsev, T. Laoui, L. Froyen, V.I. Titov, M.B. Ignatiev, Balling processes during selective laser treatment of powders, Rapid Prototyping J. 10 (2) (2004) 78–87.
[6] D.E. Bunnell, Fundamentals of Selective Laser Sintering of Metals, Ph.D. Thesis, University of Texas at Austin, Austin, TX, 1995.
[7] T. Manzur, T. DeMaria, W. Chen, C. Roychoudhuri, Potential role of high power laser diode in manufacturing, SPIE Photonics West Conference, San Jose, CA, 1996.
[8] R. Morgan, C.J. Sutcliffe, W. O'Neill, Experimental investigation of nanosecond pulsed Nd:YAG laser re-melted pre-placed powder beds, Rapid Prototyping J. 7 (3) (2001) 159–172.
[9] R. Viskanta, Phase change heat transfer, in: G.A. Lane (Ed.), Solar Heat Storage: Latent Heat Materials, CRC Press, Boca Raton, FL, 1983.
[10] L.S. Yao, J. Prusa, Melting and freezing, Adv. Heat Transfer 19 (1989) 1–95.
[11] Y. Zhang, A. Faghri, Melting of a subcooled mixed powder bed with constant heat flux heating, Int. J. Heat Mass Transfer 42 (5) (1999) 775–788.
[12] T. Chen, Y. Zhang, Analysis of melting in a mixed powder bed with finite thickness subjected to constant heat flux heating, Proceeding of ASME Summer Heat Transfer Conference, Las Vegas, NV, July 21–23, 2003.
[13] G.R. Hadley, Thermal conductivity of packed metal powders, Int. J. Heat Mass Transfer 29 (6) (1986) 909–920.